Biogeosciences Discuss., 7, 5119–5156, 2010
www.biogeosciences-discuss.net/7/5119/2010/
doi:10.5194/bgd-7-5119-2010

Biogeosciences Discussions

Calcifying invertebrates succeed in a naturally CO_2 enriched coastal habitat but are threatened by high levels of future acidification

J. Thomsen[1], M. A. Gutowska[2], J. Saphörster[1], A. Heinemann[1,3], K. Trübenbach[2], J. Fietzke[3], C. Hiebenthal[4], A. Eisenhauer[3], A. Körtzinger[5], M. Wahl[4], and F. Melzner[1]

[1]Biological Oceanography, Leibniz-Institute of Marine Sciences (IFM-GEOMAR), Kiel 24105, Germany
[2]Institute of Physiology, Christian-Albrechts-University Kiel, Germany
[3]Marine Geosystems, Leibniz-Institute of Marine Sciences (IFM-GEOMAR), Kiel 24148, Germany
[4]Marine Ecology, Leibniz-Institute of Marine Sciences (IFM-GEOMAR), Kiel 24105, Germany

[5] Chemical Oceanography, Leibniz-Institute of Marine Sciences (IFM-GEOMAR), Kiel 24105, Germany

Received: 15 June 2010 – Accepted: 22 June 2010 – Published: 2 July 2010

Correspondence to: F. Melzner (fmelzner@ifm-geomar.de)

Published by Copernicus Publications on behalf of the European Geosciences Union.

BGD
7, 5119–5156, 2010

Abstract

CO_2 emissions are leading to an acidification of the oceans. Predicting marine community vulnerability towards acidification is difficult, as adaptation processes cannot be accounted for in most experimental studies. Naturally CO_2 enriched sites thus can serve as valuable proxies for future changes in community structure. Here we describe a natural analogue site in the Western Baltic Sea. Seawater pCO_2 in Kiel Fjord is elevated for large parts of the year due to upwelling of CO_2 rich waters. Peak pCO_2 values of >230 Pa (>2300 µatm) and pH values of <7.5 are encountered during summer and autumn, average pCO_2 values are ~70 Pa (~700 µatm). In contrast to previously described naturally CO_2 enriched sites that have suggested a progressive displacement of calcifying auto- and heterotrophic species, the macrobenthic community in Kiel Fjord is dominated by calcifying invertebrates. We show that blue mussels from Kiel Fjord can maintain control rates of somatic and shell growth at a pCO_2 of 142 Pa (1400 µatm, pH=7.7). Juvenile mussel recruitment peaks during the summer months, when high water pCO_2 values of ~100 Pa (~1000 µatm) prevail. Our findings indicate that calcifying keystone species may be able to cope with surface ocean pH values projected for the end of this century. However, owing to non-linear synergistic effects of future acidification and upwelling of corrosive water, peak seawater pCO_2 in Kiel Fjord and many other productive estuarine habitats could increase to values >400 Pa (>4000 µatm). These changes will most likely affect calcification and recruitment, and increase external shell dissolution.

1 Introduction

Future ocean acidification will most likely impact ocean ecosystems by differentially modulating species fitness and biotic interactions. Decreases in pH predicted for the next century have been shown to affect several marine taxa (Fabry et al., 2008). In short to intermediate (days-weeks) CO_2 perturbation experiments, calcifying marine

BGD
7, 5119–5156, 2010

invertebrate groups have been shown to react sensitively to simulated ocean acidification (Dupont et al., 2008; Pörtner et al., 2004; Kurihara, 2008). Current hypotheses derived from experimental work suggest that there could be (i) direct effects of carbonate chemistry on calcification rate and shell integrity and that (ii) CO_2 induced disturbances in extracellular acid-base equilibria can lead to metabolic disturbances, which then impact growth and calcification rate, and, ultimately, fitness (Pörtner et al., 2004; Fabry et al., 2008; Melzner et al., 2009).

However, as most laboratory experiments cannot account for species' genetic adaptation potential, they are limited in their predictive power. Naturally CO_2 enriched habitats have thus recently gained attention as they could more accurately serve as analogues for future, more acidic ecosystems. The most prominent example, the volcanic CO_2 vents off of Ischia, Italy, have been shown to exert a negative influence on calcifying communities, with certain taxa (scleractinian corals, sea urchins, coralline algae) absent and seagrasses dominating in the acidic parts of the study site (Hall-Spencer et al., 2008). Upwelling regions could also serve as natural analogue sites. "Corrosive" upwelling of CO_2 enriched Pacific seawater onto the American shelf has recently been demonstrated (Feely et al., 2008). In shelf seas, seasonal stratification of water masses, respiration in deeper layers and subsequent upwelling of CO_2 enriched waters also results in an acidification of coastal surface waters. Our study site in the Western Baltic Sea is such a habitat: summer hypoxia and anoxia develop in bottom water layers, and strong upwelling events have been measured and modelled along the coasts (Hansen et al., 1999; Lehmann et al., 2002). However, prior to this study no detailed measurements of coastal carbonate system variability have been available for this system.

Here, we present first measurements of carbonate system variability in the shallow water habitats of Kiel Fjord. We also present field data on settlement success of invertebrate larvae and discuss growth rates of blue mussels in Kiel Fjord. Further, we conduct two laboratory experiments using the dominant benthic calcifier, the blue mussel *Mytilus edulis*, as a model species. In a first experiment (2 week duration), we

BGD
7, 5119–5156, 2010

study haemolymph ion- and acid base regulation in larger mussels to test whether this species is able to control the carbonate system speciation in its extracellular fluids. In a second experiment (8 week duration), we expose small and medium sized mussels to elevated seawater pCO_2 under an optimized feeding regime to test the hypothesis, whether disturbances in acid-base equilibria impact growth and calcification performance. We analyze shell morphology and microstructure from long-term acclimated mussels (Exp. 2) in order to determine whether formation of "control" shell material is possible under acidified conditions.

2 Material and methods

2.1 Animals

Mytilus edulis were collected from a subtidal population in Kiel Fjord (54°19.8′ N; 10°9.0′ E). For extracellular acid-base status experiments (Exp. 1), large specimens with a shell length of 76±5 mm were used. The long-term growth and calcification trial (Exp. 2) was conducted with mussels of 5.5±0.6 ("small") and 13.3±1.4 mm ("medium") shell length. Mussels were collected in March and April 2008 (acid-base regulation) and May 2009 (growth and calcification). Prior to experimentation, shells were cleaned of epibionts and animals were acclimated to the experimental settings for one to two weeks.

2.2 Experimental setup

Experiments were performed in a flow-through seawater system under a 14:10 LT light/dark cycle. Seawater from Kiel Fjord was filtered through a series of 50, 20, and 5 µm water filters, UV-sterilized and subsequently pumped at a rate of 5 l min^{-1} into a storage tank of 300 l volume. The water was aerated and mixed by a pump to ensure that air saturated water was pumped up to a header tank which supplied 12 experimental aquaria (volume=16 l each) by gravity feed. The flow rate was adjusted

BGD
7, 5119–5156, 2010

to 100 ml min^{-1} aquarium^{-1}. Overflow drain pipes in the storage tank, header tank, and every aquarium ensured constant water levels in the system. The experimental aquaria were continuously aerated using a central automatic CO_2 mixing-facility (Linde Gas & HTK Hamburg, Germany). This custom built gas-mixing facility determines the CO_2 content of inflowing ambient air and automatically adds pure CO_2 to produce five different CO_2-air mixtures. CO_2-enriched air with a pCO_2 of 57, 85, 113, 142 and 405 Pa (i.e. 385, 560, 840, 1120, 1400, 4000 µatm) was injected into the experimental aquaria at a rate of 0.8 l min^{-1} using aquarium diffuser stones (Dohse, Grafschaft-Gelsdorf, Germany). Ambient air (ca. 39 Pa/385 µatm pCO_2) was used as a control.

2.3 Experimental protocol

Exp. 1: two *M. edulis* experimental runs lasted for 14 days each at a constant water temperature of 12 °C (Exp. 1). Temperature in the storage tank was kept constant using heaters (Eheim, Deizisau, Germany) or a flow-through cooler (TITAN 1500, Aqua Medic, Bissendorf, Germany). In the first run (Exp. 1a, 29 April–16 May 2008) only the five lower pCO_2 levels were used, in the second run (Exp. 1b, 28 May–12 Juny 2008) all six levels were used. Six replicate mussels were placed in each of the experimental aquaria (biomass, total wet mass per aquarium=246±35 g). Mussels were fed with an algae suspension (DT's Live Marine Phytoplankton Premium Blend) which was pumped into the header tank using a peristaltic pump at a rate of 1 ml min^{-1} to maintain stable concentrations of 1000 to 4000 cells ml^{-1} within the experimental aquaria. Previous work established that blue mussels display maximum filtration rates when exposed to such algae densities (Riisgard et al., 2003). The algae suspension contained *Nannochloropsis oculata* (40%), *Phaeodactylum tricornutum* (40%), and *Chlorella* sp. (20%). At the end of the experimental period, animals were gently removed from the aquaria. Extracellular fluid samples were taken within two min after removal from the aquaria. Haemolymph samples of *M. edulis* were drawn anaerobically with a syringe from the posterior adductor muscle after valves were opened and blocked with a pipette

BGD
7, 5119–5156, 2010

tip. Similarly, extrapallial fluid (EPF) was sampled from the extrapallial space by gently inserting a long (ca. 6 to 7 cm) syringe needle between shell and the pallial attachment. Two samples were taken from each animal. The first sample (200 µl) was used for pH determination and the second (500 µl) for measurement of total dissolved inorganic carbon (C_T) and ion composition (see below). Water samples were taken from the aquaria for the determination of ionic composition, A_T, and C_T

Exp. 2: in a long-term growth experiment, mussels were exposed for 2 months to three pCO_2 levels (39, 142, and 405 Pa/385, 1400, 4000 µatm) in four replicate aquaria for each treatment level at a mean temperature of 13.8±0.6 °C between 14 May–13 July 2009. Each replicate contained eight mussels of 5.5 mm ("small") and 13 mm ("medium") shell length. Initial total biomass per replicate aquarium was 14±0.5 g. Mussels were continuously fed with a *Rhodomonas* sp. suspension containing 2903±1194 cells ml^{-1} which was introduced into each aquarium at a rate of 100 ml min^{-1}. *Rhodomonas* sp. was cultured in 0.2 µm filtered seawater enriched with Provasolis seawater medium (Ismar et al., 2008), phosphate, and nitrate at a final concentration of 0.036 mmol l^{-1} P and 0.55 mmol l^{-1} N in plastic bags at 7.5 l each under constant illumination. Mean algae concentrations in the experimental aquaria were 820±315 cell ml^{-1}. Shell length and fresh mass of the mussels were measured at the beginning of the experiment and after 8 weeks using a calliper (±0.1 mm) and a precision balance (±1 mg). Somatic dry and shell mass were measured after drying the animals for 24 h at 80 °C using a precision balance (±1 mg, Sartorius, Germany). Similar determinations were carried out for control mussels from Kiel Fjord collected at the sampling site of our experimental animals.

2.4 Determination of carbonate system parameters

Daily measurements were conducted to monitor pH, salinity, and temperature in the aquaria and the same parameters were determined weekly in Kiel Fjord (54°19.8′ N; 10°9.0′ E). pH was measured with a WTW 340i pH-meter and a WTW SenTix 81-electrode which was calibrated with Radiometer IUPAC precision pH buffer 7 and 10

BGD
7, 5119–5156, 2010

(S11M44, S11 M007). Salinity and temperature were measured with a WTW cond 315i salinometer and a WTW TETRACON 325 probe. Water samples from the aquaria and Kiel Fjord were taken for determination of total alkalinity (A_T) and total dissolved inorganic carbon (C_T). A_T was measured by means of a potentiometric open-cell titration with hydrochloric acid using a VINDTA autoanalyzer (Mintrop et al., 2000; Dickson et al., 2007). C_T was determined coulometrically (Dickson et al., 2007) using a SOMMA autoanalyzer. Both A_T and C_T measurements were measured against Certified Reference Material provided by Andrew Dickson of the Scripps Institution of Oceanography (http://andrew.ucsd.edu/co2qc/) yielding an overall precision (accuracy) of about 1 (2) µmol kg^{-1} and 1.5 (3) µmol kg^{-1}, respectively. Seawater carbonate system parameters (Ω, pCO_2) were calculated using the CO2sys program (Dickson et al., 2003; Lewis and Wallace, 1998). Dissociation constants K_1 and K_2 (Mehrbach et al., 1973; Dickson and Millero, 1987), $KHSO_4$ dissociation constant (Dickson, 1990) and the NBS scale [mol kg^{-1} H_2O] were used. The measured pH_{NBS} values of the experiments were corrected by a correlation of pH_{NBS} calculated from A_T and C_T for every experiment. Kiel Fjord surface pCO_2 values were estimated from weekly measured pH_{NBS} values (42 weeks between 01 April 2008 and 01 April 2009). For this purpose, measured pH_{NBS} was correlated with pCO_2 values calculated from measured A_T and C_T values (Eq. 1, n=9, see Table 1 for A_T and C_T values, r^2=0.94):

$$pCO_2 = -281.14 pH_{NBS} + 2291.3, \quad (1)$$

where pCO_2 is the seawater pCO_2 in Pa, pH_{NBS} is the measured seawater pH value.

2.5 Determination of extracellular acid-base and ion status

In Exp. 1a, *M. edulis* haemolymph (HL) pH_{NBS} was measured in a 12 °C water bath using fiber-optic sensors (optodes, PreSens, Regensburg, Germany) which were installed in the tip of 1 ml syringes (Gutowska and Melzner, 2009). Samples were filtered through a glassfiber filter at the syringe tip to remove haemocytes. The sensors were calibrated in ambient sea water which was adjusted to four different pH_{NBS} values

BGD
7, 5119–5156, 2010

between 6.9 and 7.8 with HCl and NaOH. Optodes were calibrated against a WTW 340i pH meter and a SenTix 81 electrode, calibrated with Radiometer precision buffers (S11M44, S11 M007). In Exp. 1b, pH_e was measured within a cap using a microelectrode (WTW Mic-D) and a WTW 340i pH meter. The slight offset of the WTW pH_{NBS} electrodes with respect to pH_{NBS} values calculated from A_T and C_T measurements on the same water bodies were corrected by using the following linear relationship (Eq. (2), n=95, r^2=0.96):

$$pH_{corrected} = 0.9398 pH_{measured} + 0.556 . \quad (2)$$

Haemolymph C_T was measured in two 100 µl subsamples with a Corning 965 CO_2 analyzer. To correct for instrument drift 100 µl of distilled water were measured prior to each sample determination. Thus, a precision and accuracy of 0.1 mM could be reached. To determine in vitro non-bicarbonate buffer (NBB) – values of extracellular fluid, 600 µl samples pooled from 10 animals were equilibrated with humidified CO_2 gas mixtures (pCO_2 57, 142, 405, 564 Pa/560, 1400, 4000, 5570 µatm) for 1 h using the gas mixing facility and a gas mixing pump (Wösthoff, Bochum, Germany). Incubations were performed in a shaking water bath at 12 °C, using glass flasks (120 ml) as incubators. pH_{NBS} and C_T were measured using a microelectrode (WTW Mic-D) and Corning 965 CO_2 analyzer, respectively, as described above.

Body fluid pCO_2, bicarbonate, and carbonate concentrations were calculated from measured pH and C_T values according to the rearranged versions of the Henderson-Hasselbalch equation:

$$pCO_2 = C_T \left(10^{ph - pK_1'} \alpha_{CO_2} + \alpha_{CO_2}\right)^{-1} \quad (3)$$

$$\left[HCO_3^{2-}\right] = 10^{pH - pK_1'} \alpha_{CO_2} pCO_2 \quad (4)$$

$$\left[CO_3^{2-}\right] = 10^{pH - pK_2'} \left[HCO_3^-\right] \quad (5)$$

BGD
7, 5119–5156, 2010

where α is the CO_2 solubility coefficient and pK_1' and pK_2' are the first and second apparent dissociation constants of carbonic acid. α_{CO_2} was calculated (Weiss, 1974) and pK_2' (Roy et al., 1993) was chosen according to experimental temperature and salinity. pK_1' was calculated from pH_{NBS}, C_T, and pCO_2 measured in vitro in body fluids of both species using Eq. (6) (Albers and Pleschka, 1967):

$$pK_1' = pH - \log\left(\frac{C_T}{pCO_2\alpha_{CO_2}} - 1\right). \quad (6)$$

A linear relationship was found for pK_1' in relation to pH_{NBS}. The regression for pK_1' for *M. edulis* haemolymph was $pK_1' = -0.1795\,pH + 7.5583$ ($r^2 = 0.5$). The calculated values for pK_1' in *M. edulis* differed between 6.20±0.03 in control and 6.27±0.02 in 405 Pa pCO_2 treated animals. Protein concentration in the haemolymph was determined using a Thermo Multiskan spectrum photometer (Waltham, Massachusetts, USA) and BSA standard solutions (Bradford, 1976). Prior to measurements samples were centrifuged to remove haemocytes (100 g, 25 min, 2 °C). The total cation concentrations of water and body fluid were measured using a Dionex ICS-2000 ion chromatograph, a CS18 column and methane sulfonic acid as eluent. Samples were centrifuged for 20 min at 100 g and 4 °C to remove haemocytes. The supernatant was transferred into a new cap and frozen at −20 °C. Prior to measurement, body fluid and ambient seawater samples were diluted 1:100 with de-ionized water. A calibration curve was obtained by measuring a dilution series of 1:50, 1:100, 1:200, 1:300, 1:400, and 1:500 of the IAPSO seawater standard (International Association for the Physical Sciences of the Oceans, batch: P146; 12 May 2005; salinity:34.992; K15:0.99979).

2.6 Larval settlement in Kiel Fjord

Monthly, settlement substrata were exposed to natural colonization at the IFM-GEOMAR pier at a depth of 1 m, approximately 50 m north of the carbonate chemistry sampling site. Settlement substrata were made of grey PVC manually roughed using

BGD
7, 5119–5156, 2010

grain 60 sandpaper to facilitate attachment. Each unit consisted of three differently oriented, 5 cm×5 cm surfaces: vertical, horizontal upwards, horizontal downwards. The units were allowed to rotate freely around their vertical axis. The use of a biologically widely accepted material and the different orientations in space maximized our capacity to sample a large proportion of the propagules settling in a particular month. After retrieving the substrata at the end of a 4-week-exposure, they were gently rinsed to remove unattached organisms, then foulers were identified to the lowest taxonomic level possible (genus or species), and % cover per taxon was estimated. The level of replication was three.

2.7 Mussel shell growth using $MnCl_2$ as a marker

Individually tagged young (13 to 22 mm) blue mussels (*M. edulis*) from Kiel Fjord were placed into a net on 31 January 2007 and subsequently submerged into a container containing ambient seawater supplemented with 20 mg l^{-1} $MnCl_2$ for 6 to 24 h (with breaks from 26 July 2007 to 23 August 2007, from 07 November 2007 to 29 November 2007 and from 19 December 2007 to 10 January 2008). In these treatment phases, the mussels incorporated manganese during precipitation of their shells (Barbin et al., 2008). The days between the $MnCl_2$ markings the mussel net was freely suspended at the IFM-GEOMAR jetty in Kiel Fjord at about 1 m water depth, enabling the mussels to filter feed in their natural environment. After 12 months (on 05 February 2008) the soft tissue of the mussels was removed and the left valve of one individual (initial shell length: 16.1 mm, final shell length: 46.6 mm) was prepared for electron micro probe (EMP) measurements: The shell was cut along the axis of maximum growth using a cut-off wheel and shell sections were embedded in a two component epoxy resin (Buehler, EPO-THIN, Low Viscosity Epoxy Resin) on a brass-slide. After hardening at 50 °C, the sections were ground with sand paper (grading (*p*):240 to 600) and polished with diamond paste (grading 0.5 to 0.01 µm). EMP analyses were carried out at IFM-GEOMAR Kiel, Germany, using a JEOL JXA 8200 "Superprobe" applying Wavelength Dispersive Spectrometry (WDS), using a focused beam, a resolution between

BGD
7, 5119–5156, 2010

3 µm×3 µm and 10 µm×10 µm and an integration time per point of 400 ms.

2.8 Shell morphology and shell microstructure

Shell morphology was assessed for 20 randomly chosen, medium sized mussels from each treatment in experiment 2. Mussel shells were checked for external and internal shell dissolution under low magnification (8 times magnification) using a stereomicroscope. Shell umbones were photographed at 18 times magnification and analyzed for signs of external dissolution (50 times magnification). Images were analyzed for the extent of dissolution at the umbo with an accuracy of 1 mm^2 (the large uncertainty is due to the curvature of the shell). Severity of dissolution was graded according to the following scale, the "dissolution index": 0=no dissolution, 1=periostracum abrasion, 2=calcite dissolution visible, 3=massive dissolution of calcite, multi-layered, often with round dissolution pits. Other dissolution spots on the outer shell surface were not quantified.

Microstructure of shell cross sections at two different positions of the shell of randomly chosen *M. edulis* (n=5) from experiment 2 (medium size) that were characterized by similar final shell lengths was investigated. Shells were perforated every 2 mm along the longitudinal axis (i.e. anterior-posterior axis) using a 1 mm diameter drill. They could then be manually fractured in a controlled fashion. Shell analysis was performed exclusively on intact cross sections in between drilled holes. We found that such a procedure produces high quality cross sections. Position one (at 75% shell length) is located anterior to the pallial line (PL) and consists of aragonite and calcite layers. Position two (at 95% shell length) lies posterior to the PL and is solely composed of calcite. Both positions are located in shell regions formed during the experiment. The shell fractions were coated with gold-palladium and examined using scanning electron microscopy (SEM, Nanolab 7, Zeiss). The thickness of the different crystal layers (aragonite, calcite) and the number of the aragonite platelets were quantified.

BGD
7, 5119–5156, 2010

2.9 Statistical analyses

Regression analysis was performed with SigmaPlot 10. Statistical analyses were performed using STATISTICA 8. Differences between treatments were analyzed using one- and two-way ANOVA and the Tukey post-hoc test for unequal *n*. Relative quantities were arcsine transformed prior to analysis. For shell morphology analysis of dissolved shell area and the dissolution index, non-parametric Kruskal-Wallis and subsequent Dunn's Multiple Comparisons Tests were used. Values in graphs and tables are means ± standard deviation.

3 Results and discussion

3.1 Habitat carbonate system speciation and calcifying communities

The western Baltic Sea is characterized by a low salinity (10 to 20) and relatively low A_T of 1900 to 2150 µmol kg^{-1}. Thus, the calcium carbonate saturation state (Ω) typically is much lower than in the open ocean. Our A_T and C_T measurements in 2008 and 2009 indicate that Ω_{arag} did not exceed a value of one in Kiel Fjord surface waters during summer and autumn. Even Ω_{calc} dropped below one on multiple occasions (Table 1, Fig. 1a). Minimum values for Ω_{arag} (Ω_{calc}) were 0.35 (0.58) in September 2008. Low Ω is associated with high surface pCO_2 during the summer and autumn months, caused by upwelling of CO_2-rich deeper water masses (Hansen et al., 1999). Kiel Fjord surface pCO_2 exceeds present average ocean pCO_2 values during large parts of the year. Habitat pCO_2 varies between 38 and 234 Pa (375 and 2309 µatm), pH_{NBS} varies between 7.49 and 8.23. Using a correlation of weekly measured surface pH_{NBS} and calculated pCO_2 from A_T and C_T measurements, we estimate that in 34%, 23% and 9% of 42 weeks investigated, pCO_2 exceeded pre-industrial pCO_2 (28 Pa, 280 µatm) by a factor of three (>85 Pa, >840 µatm), four (>113 Pa, >1120 µatm) and five (>142 Pa, >1400 µatm), respectively.

BGD
7, 5119–5156, 2010

Given the particular carbonate system variability of the habitat it is surprising that blue mussel (*Mytilus edulis*) beds and associated calcifying benthic species (e.g. the barnacle *Amphibalanus improvisus*, the echinoderm *Asterias rubens*) are common features in Kiel Fjord and the Western Baltic. *M. edulis* forms a shell consisting of an inner aragonite (nacre) and outer calcite layer, covered and protected by an organic layer, the periostracum. Despite an extensive organic matrix surrounding the calcite and aragonite crystals, 95–99.9% of the shell's mass is comprised of $CaCO_3$ (Yin et al., 2005). *M. edulis* constitutes more than 90% of the macrofauna biomass in many habitats in the Western Baltic (Reusch and Chapman, 1997; Enderlein and Wahl, 2004). Competitive dominance is achieved primarily through very high rates of recruitment (spatfall) and high rates of juvenile growth (Dürr and Wahl, 2004). Previous results indicate that *M. edulis* (2 to 3 cm shell length) are characterized by shell growth rates of ca. 4 mm month^{-1} during the summer months in Kiel Fjord (Kossak, 2006). Our EMP analysis of a $MnCl_2$ marked mussel confirms these earlier findings and indicates that weekly shell increments in the field can exceed 1 mm week^{-1} during May to October (Fig. 2). Settlement of juvenile mussels in 2008 occurred exactly when highest pCO_2 values were encountered in the habitat (Fig. 1c): peak settlement took place in July and August, at an average surface pCO_2 of 98 Pa (967 µatm). Other calcifying invertebrates (e.g. the barnacle *Amphibalanus improvisus*) also settled abundantly between May and October 2008 in Kiel Fjord (Fig. 1c). When settlement plates are not exchanged regularly, mussels have been found to dominate the species assemblage (>0.99 by biomass) in Kiel Fjord within ~10 weeks in summer (Enderlein and Wahl, 2004).

3.2 *M. edulis* extracellular acid-base status (Exp. 1)

In order to better understand the success of *M. edulis* in Kiel Fjord, a chemically and physiologically challenging habitat, we studied haemolymph pH_{NBS} (pH_e) and ion regulation (Exp. 1) and, subsequently growth and calcification performance (Exp. 2). In Exp. 1 we acclimated mussels to six pCO_2 values between 39 and 405 Pa (385 to

BGD
7, 5119–5156, 2010

4000 µatm) in a flow-through seawater system for a period of two weeks (see Table 2 for sea water chemistry) to then obtain haemolymph samples. We found that mussels do not regulate pH_e when exposed to elevated seawater pCO_2. pH_e followed the non-bicarbonate buffer line when displayed in a Davenport-diagram (Fig. 3, Table 3), suggesting that buffering by extracellular proteins (1.2 ± 0.4 mg mL^{-1}, N=8 control mussels) is the sole mechanism to stabilize pH_e. The buffer value of the haemolymph is low (0.49 mM HCO_3^- pH^{-1}, Fig. 3), matching findings from other populations of the same species (Booth et al., 1984; Lindinger et al., 1984). Significant reductions in pH_e were found at 142 and 405 Pa (Table 3, Fig. 3a). No significant changes in the concentration of haemolymph Mg^{2+} and Ca^{2+} were observed with respect to treatment pCO_2 (Table 3). While it was proposed that mytilid mussels use HCO_3^- derived from their shells to buffer pH_e (Lindinger et al., 1984; Michaelidis et al., 2005), our results clearly demonstrate that in flow-through seawater experimental designs, *M. edulis* do not maintain extracellular [HCO_3^-] above that of ambient seawater. This is in contrast to the more active cephalopod molluscs, which greatly elevate extracellular [HCO_3^-] in order to stabilize pH_e to conserve haemocyanin blood oxygen transport (Gutowska et al., 2010). However, while *M. edulis* does not possess a pH sensitive respiratory pigment, uncompensated pH_e might negatively impact shell formation: comparing control extracellular pH of haemolymph drawn from the posterior adductor muscle with that of the extrapallial fluid (EPF), the fluid that fills the space between mantle and shell surface, indicates that both fluids are characterized by a very similar carbonate system speciation (Table 3B). Assuming that pH_e in the EPF always behaves like that of haemolymph, it is very likely that the inner shell layers (nacre), which primarily consist of aragonite, are in contact with a fluid that is highly under saturated with $CaCO_3$: haemolymph [CO_3^{2-}] is much lower than in seawater [CO_3^{2-}] at any given seawater pCO_2 (see Fig. 3b). As in addition, only 15% of total EPF [Ca^{2+}] has been found to be freely dissolved Ca^{2+} (Misogianes and Chasteen, 1979), Ω_{arag} would be even lower at the inner shell interface.

BGD
7, 5119–5156, 2010

3.3 *M. edulis* growth and calcification (Exp. 2)

To estimate the long-term repercussions of decreased pH_e on the energy budget and the calcification machinery, we conducted a growth trial under optimized feeding conditions (Exp. 2). Previous studies suggested that in mytilid bivalves (*M. galloprovincialis*), uncompensated reductions in pH_e may be causally related to reductions in metabolism (metabolic depression) and somatic growth (Michaelidis et al., 2005). In our 8 week growth study, shell length growth was high under control conditions (3.3 to 4.6 mm month^{-1} in small vs. medium mussels), fully matching summer field growth rates for mussels of the same size classes in Kiel Fjord (Kossak, 2006). Initial mussel shell length and pCO_2 had significant effects on shell length growth and shell mass increment (see Table 4 for ANOVA results). While shell mass and length growth were similar in control and 142 Pa treated medium sized mussels, both parameters were significantly reduced at 405 Pa (Fig. 4a). In the smaller size group, length growth was significantly reduced at 405 Pa as well. There were no significant differences in shell mass growth in small mussels, although a trend towards lower shell mass was apparent in the 405 Pa group as well (Fig. 4b). However, when displaying shell mass vs. shell length in comparison to wild-type mussels collected from the sampling site in Kiel Fjord (grey symbols in Fig. 4a,b), it appears that all experimental groups lie within the 95% prediction band of the shell mass vs. length function. This indicates that exposure to elevated pCO_2 does not result in the production of a grossly abnormal, thinner shell phenotype; rather, shell growth is slowed proportionally. Regardless of the decreased rates of shell growth at higher pCO_2 (405 Pa), all treatment mussels increased their shell mass at least by 150% during the 8 week trial, even at Ω_{arag} (Ω_{calc}) as low as 0.17 (0.28) (Fig. 4e). This is in contrast to a previous study that has suggested a high sensitivity of mussel calcification to elevated pCO_2: during acute exposure, a linear correlation between $CaCO_3$ precipitation rate and seawater pCO_2 (and $[CO_3^{2-}]$) has been observed in *M. edulis* from the Western Scheldt. A reduction in calcification by about 50% was found at a pCO_2 of ca. 100 Pa (ca. 1000 µatm), net shell dissolution was ob-

BGD
7, 5119–5156, 2010

served at pCO_2 higher than ca. 180 Pa (ca. 1800 µatm, Gazeau et al., 2007). Clearly, acclimation, adaptation and food availability or quality could be responsible factors for the observed differences between both studies. Somatic growth was not significantly affected by pCO_2 in our experiment (Fig. 4f). This may primarily be due to high variability encountered between replicates, but also could point at a higher capacity for somatic growth vs. shell accretion under hypercapnic conditions. Findings pointing in this direction have recently been obtained for an echinoderm species, where somatic growth was up-regulated under acidified conditions while calcification was suppressed (Gooding et al., 2009).

3.4 *M. edulis* shell microstructure and morphology (Exp. 2)

SEM analyses of shell cross-sections from mussels with a similar final length from all growth trial treatments (Table 5), illustrates that there are no significant changes in calcite and aragonite layer thickness in newly formed shell parts when pCO_2 is elevated. While calcite layer thickness is also comparable between 39 Pa and 405 Pa mussels, a significant decrease in the thickness of individual aragonite platelet layers, from 0.6 to 0.38 µm, was evident in the 405 Pa treatment. This indicates that high levels of acidification result in changes in shell microstructure that are not detected by simple shell mass vs. shell length regression analysis. As mentioned above, it needs to be emphasized that nacre (aragonite) platelet layers on the inner side of the shell (Fig. 4c) are in contact with an extrapallial fluid (EPF) that is most likely characterized by Ω_{arag} of <0.4 even under control conditions. Our shell microstructure analysis (Table 5) indicates that even at 405 Pa, the same number of aragonite platelets can be formed as in control animals of the same length. Thus, mussels must possess a powerful calcification machinery to construct and maintain shell integrity in an EPF that is highly under saturated with $CaCO_3$.

M. edulis seems to be well adapted to form shell material even under highly acidified conditions when the newly formed material is protected by an intact periostracum. However, fractures of the periostracum seem to be fairly common, even in control mus-

BGD
7, 5119–5156, 2010

sels and especially at the umbo region and other older parts of the shell (Fig. 5). Mussels occur in dense beds in Kiel Fjord (see Fig. 1d) and the umbo region is often in close contact to other mussels or the substrate. Friction in a wave swept environment then probably causes an abrasion of the organic cover. Such fractures can then act as nucleation sites for external shell dissolution. We found some degree of periostracum damage and/or shell dissolution at the umbo region in 58 out of 60 medium sized mussels analyzed from Exp. 2. Dissolution area was smallest (<2 mm^2) in control mussels and significantly increased at 142 and 405 Pa (Fig. 6a). While shell damage was primarily restricted to periostracum abrasion in the control group (dissolution index=1, Fig. 5a), significantly more calcite dissolution was observed in the 405 Pa group (dissolution index=3, Figs. 5c, 6b). Dissolution spots (e.g. Fig. 7) could be demonstrated in a range of mussels at 39, 142 and 405 Pa, mainly in old parts of the shell, indicating that periostracum damage and subsequent external dissolution also occurs in the natural habitat (Fig. 7a–f). As we did not screen our experimental mussels for periostracum damage prior to the experiment incubation, it is difficult to assess the magnitude of shell dissolution during the incubation. In two mussels (one at 142 Pa, one at 405 Pa), dissolution spots could also be witnessed in newly formed shell parts (Fig. 7c,g–i). It is unclear, whether elevated seawater pCO_2 itself can disrupt the protective function of the periostracum. Future studies need to take this possibility into consideration.

4 Conclusions

In summary, our laboratory studies demonstrate that calcification in this economically and ecologically important bivalve species can be maintained at control rates even when seawater Ω_{arag} is lower than 0.5 (pCO_2 142 Pa, 1400 µatm). 56 to 65% of control calcification rates can be obtained at a seawater pCO_2 of 405 Pa (4000 µatm), a pCO_2 that is twice as high as that producing zero calcification in an already mentioned acute study on a North Sea population (Gazeau et al., 2007). This could be due to physiological differences between North- and Baltic Sea populations of *M. edulis*; however, our

BGD
7, 5119–5156, 2010

and other studies indicate that it is more likely that long-term acclimation to elevated pCO_2 increases the ability to calcify in *Mytilus* spp. (Michaelidis et al., 2005; Ries et al., 2009). We also show evidence that uncompensated extracellular pH at moderately elevated pCO_2 (142 Pa, 1400 µatm) does not significantly impair growth and calcification, suggesting that there is no causal relationship between acid-base status and metabolic depression in this species at levels of ocean acidification that can be expected in the next few hundred years (IPCC, 2007). Rather, we show in a companion study that moderate levels of acidification (pCO_2 113 to 240 Pa, 1120 to 2400 µatm) increase metabolic rates, potentially indicating increased costs for calcification and cellular homeostasis (Thomsen and Melzner, 2010).

While current levels of CO_2 enrichment may still permit the dominance of calcifying communities in habitats such as Kiel Fjord, future increases in pCO_2 could deplete their tolerance capacity: an increase in seawater pCO_2 from 39 to 78 Pa (385 to 770 µatm) due to future ocean acidification will elevate C_T by approximately 90 µmol kg^{-1} (i.e. at S=20, A_T=2060 µmol kg^{-1}, T=20 °C), but leave A_T unaffected. Simple model calculations illustrate, how additional increases in C_T due to respiration in deeper water masses and subsequent upwelling would affect the carbonate system speciation in Kiel Fjord (Fig. 1b): adding 100 µmol kg^{-1} of C_T to the values measured in 2008 and 2009 (see Table 1) and leaving A_T unaltered results in dramatic increases in pCO_2; Peak pCO_2 values would shift from ca. 230 to >440 Pa (>4300 µatm), average pCO_2 for the measurements in Table 1 would shift from ca. 104 Pa to 248 Pa (2450 µatm). As pCO_2 is generally highest in the summer months, mussel recruitment could be one of the first processes to be affected: Kurihara and colleagues (Kurihara et al., 2009) demonstrated a high CO_2 sensitivity of larval *M. galloprovincialis*, with an increased prevalence of shell malformation at a pCO_2 of ca. 200 Pa (ca. 2000 µatm). Such values could be reached within the next decades in Kiel Bay (Fig. 1b). However, older mussels would probably be affected just as well: considering that abrasions of the periostracum are very common among *M. edulis* in Kiel Fjord, enhanced external shell dissolution may compromise fitness of older mussels during long-term exposure to seawater highly un-

BGD
7, 5119–5156, 2010

der saturated with $CaCO_3$ by negatively influencing shell stability. In addition, increased external shell dissolution might favour settlement of the shell boring polychaete *Polydora ciliata* which can more easily penetrate shell parts with damaged periostracum (Michaelis, 1978). *P. ciliata* boring may render mollusc shells more vulnerable to crab predation (Blöcher 2008). In addition, invasion of the extracellular space by microorganisms through minute shell fractures seems possible. Long-term experiments (>6 months) are necessary to test these hypotheses.

Coastal upwelling habitats such as Kiel Bay or the West coast of the United States (Feely et al., 2008) can be important "natural analogues" to understand how ecosystems might be influenced by future ocean acidification. In contrast to a natural analogue study that shows a progressive displacement of calcifying organisms by photoautotrophic communities along a CO_2 gradient in the Mediterranean (Hall-Spencer et al., 2008), we show that communities dominated by calcifying invertebrates can thrive in CO_2 enriched (eutrophic, "energy dense") coastal areas. However, such habitats, which are quite common along the world's coasts (Diaz and Rosenberg, 2008), will be exposed to rates of change in seawater pCO_2 that go well beyond the worst scenarios predicted for surface oceans (Caldeira and Wickett, 2003).

Acknowledgements. The authors wish to thank Ulrike Panknin for culturing algae, supervising the long-term experiment, and laboratory work associated with this project, Hans-Ulrik Riisgard (University of Southern Denmark) for his suggestion on how to improve filtration efficiency and experimental design, Renate Schütt for marking mussels with $MnCl_2$ and carrying out the settlement plate work and Susann Grobe for carbonate chemistry analysis. This study was funded by DFG Excellence Cluster "Future ocean" grants to AK, FM and MW, This work is a contribution to the German Ministry of Education and Research (BMBF) funded project "Biological Impacts of Ocean ACIDification"(BIOACID) subproject 3.1.3 awarded to FM and MAG and is a contribution to the "European Project on Ocean Acidification" (EPOCA) that received funding from the European Community's Seventh Framework Programme (FP7/2007 to 2013) under grant agreement no 211384.

BGD
7, 5119–5156, 2010

References

Albers, C. and Pleschka, K.: Effect of temperature on CO_2 transport in elasmobranch blood, Resp. Physiol., 2, 261–273, 1967.

Barbin, V., Ramseyer, K., and Elfman, M.: Biological record of added manganese in seawater: a new efficient tool to mark in vivo growth lines in the oyster species *Crassostrea gigas*, Int. J. Earth Sci., 97, 193–199, 2008.

Blöcher, N.: Ökologische und biologische Aspekte des *Polydora ciliata*-Aufwuchses auf *Littorina littorea*, M. Sc. thesis, University of Kiel, 2008.

Booth, C. E., McDonald, D. G., and Walsh, P. J.: Acid-base-balance in the sea mussel, *Mytilus edulis*, 1. Effects of hypoxia and air-exposure on hemolymph acid-base status, Mar. Biol. Lett., 5, 347–358, 1984.

Bradford, M. M.: Rapid and sensitive method for quantitation of microgram quantities of protein utilizing principle of protein-dye binding, Ana. Biochem., 72, 248–254, 1976.

Caldeira, K. and Wickett, M. E.: Anthropogenic carbon and ocean pH, Nature, 425, 365–365, 2003.

Diaz, R. J. and Rosenberg, R.: Spreading dead zones and consequences for marine ecosystems, Science, 321, 926–929, 2008.

Dickson, A. G. and Millero, F. J.: A comparison of the equilibrium-constants for the dissociation of carbonic-acid in seawater media, Deep-Sea Res., 34, 1733–1743, 1987.

Dickson, A. G.: Standard potential of the reaction $AgCl_s + 1/2H_{2g} = Ag_s + HCl_{aq}$ and the standard acidity constant of the ion HSO_4^- in synthetic sea-water from 273.15 K to 318.15 K, J. Chem. Thermodyn., 22, 113–127, 1990.

Dickson, A. G., Afghan, J. D., and Anderson, G. C.: Reference materials for oceanic CO_2 analysis: a method for the certification of total alkalinity, Mar. Chem, 80, 185–197, 2003.

Dickson, A. G., Sabine, C. L., and Christian, J. R.: Guide to best Practices for Ocean CO_2 Measurements, PICES Special Publications, 191 pp., 2007.

Dupont, S., Havenhand, J., Thorndyke, W., Peck, L., and Thorndyke, M.: Near-future level of CO_2-driven ocean acidification radically affects larval survival and development in the brittlestar *Ophiothrix fragilis*, Mar. Ecol.-Prog. Ser., 373, 285–294, 2008.

Dürr, S. and Wahl, M.: Isolated and combined impacts of blue mussels (*Mytilus edulis*) and barnacles (*Balanus improvisus*) on structure and diversity of a fouling community, J. Exp. Mar. Biol. and Ecol., 306, 181–195, 2004.

BGD
7, 5119–5156, 2010

Enderlein, P. and Wahl, M.: Dominance of blue mussels versus consumer-mediated enhancement of benthic diversity, J. Sea Res., 51, 145–155, 2004.
Fabry, V. J., Seibel, B. A., Feely, R. A., and Orr, J. C.: Impacts of ocean acidification on marine fauna and ecosystem processes, Ices J. Mar. Sci., 65, 414–432, 2008.
Feely, R. A., Sabine, C. L., Hernandez-Ayon, J. M., Ianson, D., and Hales, B.: Evidence for upwelling of corrosive "acidified" water onto the continental shelf, Science, 320, 1490–1492, 2008.
Gazeau, F., Quiblier, C., Jansen, J. M., Gattuso, J. P., Middelburg, J. J., and Heip, C. H. R.: Impact of elevated CO_2 on shellfish calcification, Geophys. Res. Lett., 34, L07603, doi:10.1029/2006GL028554, 2007.
Gooding, R. A., Harley, C. D. G., and Tang, E.: Elevated water temperature and carbon dioxide concentration increase the growth of a keystone echinoderm, P. Natl. Acad. Sci. USA, 106, 9316–9321, 2009.
Gutowska, M. A. and Melzner, F.: Abiotic conditions in cephalopod (*Sepia officinalis*) eggs: embryonic development at low pH and high pCO_2, Mar. Biol., 156, 515–519, 2009.
Gutowska, M. A., Melzner, F., Langenbuch, M., Bock, C., Claireaux, G., and Portner, H. O.: Acid-base regulatory ability of the cephalopod (*Sepia officinalis*) in response to environmental hypercapnia, J. Comp. Physiol. B, 180, 323–335, 2010.
Hall-Spencer, J. M., Rodolfo-Metalpa, R., Martin, S., Ransome, E., Fine, M., Turner, S. M., Rowley, S. J., Tedesco, D., and Buia, M. C.: Volcanic carbon dioxide vents show ecosystem effects of ocean acidification, Nature, 454, 96–99, 2008.
Hansen, H. P., Giesenhagen, H. C., and Behrends, G.: Seasonal and long-term control of bottom-water oxygen deficiency in a stratified shallow-water coastal system, Ices J. Mar. Sci., 56, 65–71, 1999.
IPCC: Climate Change 2007: The Physical Science Basis. Contribution of Working Group I to the Fourth Assessment Report of the Intergovernmental Panel on Climate Change, Cambridge University Press, Cambridge, United Kingdom and New York, NY, USA., 2007.
Ismar, S. M. H., Hansen, T., and Sommer, U.: Effect of food concentration and type of diet on *Acartia* survival and naupliar development, Mar. Biol., 154, 335–343, 2008.
Kossak, U.: How climate change translates into ecological change: Impacts of warming and desalination on prey properties and predator-prey interactions in the Baltic Sea, Ph.D. dissertation, IFM-GEOMAR, Christian-Albrechts-Universität, Kiel, 97 pp., 2006.
Kurihara, H.: Effects of CO_2-driven ocean acidification on the early developmental stages of

BGD
7, 5119–5156, 2010

invertebrates, Mar. Ecol.-Prog. Ser., 373, 275–284, 2008.
Kurihara, H., Asai, T., Kato, S., and Ishimatsu, A.: Effects of elevated pCO_2 on early development in the mussel Mytilus galloprovincialis, Aquat. Biol., 4, 225–233, 2009.
Lehmann, A., Krauss, W., and Hinrichsen, H. H.: Effects of remote and local atmospheric forcing on circulation and upwelling in the Baltic Sea, Tellus A, 54, 299–316, 2002.
Lindinger, M. I., Lauren, D. J., and McDonald, D. G.: Acid-base-balance in the sea mussel, *Mytilus edulis*, 3. Effects of environmental hypercapnia on intracellular and extracellular acid-base-balance, Mar. Biol. Lett., 5, 371–381, 1984.
Mehrbach, C., Culberso, C. H., Hawley, J. E., and Pytkowic, R. M.: Measurement of apparent dissociation-constants of carbonic-acid in seawater at atmospheric-pressure, Limnol. Oceanogr., 18, 897–907, 1973.
Melzner, F., Gutowska, M. A., Langenbuch, M., Dupont, S., Lucassen, M., Thorndyke, M. C., Bleich, M., and Pörtner, H.-O.: Physiological basis for high CO_2 tolerance in marine ectothermic animals: pre-adaptation through lifestyle and ontogeny?, Biogeosciences, 6, 2313–2331, doi:10.5194/bg-6-2313-2009, 2009.
Michaelidis, B., Ouzounis, C., Paleras, A., and Pörtner, H. O.: Effects of long-term moderate hypercapnia on acid-base balance and growth rate in marine mussels *Mytilus galloprovincialis*, Mar. Ecol.-Prog. Ser., 293, 109–118, 2005.
Michaelis, M.: Zur Morphologie und Ökologie von *Polydora ciliata* und *P. ligni* (*Polychaeta*, *Spionidae*), Helgoländer wiss. Meeresunters., 31, 102–116, 1978.
Mintrop, L., Perez, F. F., Gonzalez-Davila, M., Santana-Casiano, M. J., and Körtzinger, A.: Alkalinity determination by potentiometry: Intercalibration using three different methods, Cienc. Mar., 26, 23–37, 2000.
Misogianes, M. J. and Chasteen, N. D.: Chemical and spectral characterization of the extrapallial fluid of *Mytilus edulis*, Anal. Biochem., 100, 324–334, 1979.
Pörtner, H. O., Langenbuch, M., and Reipschläger, A.: Biological impact of elevated ocean CO_2 concentrations: lessons from animal physiology and earth history, J. Oceanogr., 60, 705–718, 2004.
Reusch, T. B. H. and Chapman, A. R. O.: Persistence and space occupancy by subtidal blue mussel patches, Ecol. Monogr., 67, 65–87, 1997.
Ries, J. B., Cohen, A. L., and McCorkle, D. C.: Marine calcifiers exhibit mixed responses to CO_2-induced ocean acidification, Geology, 37, 1131–1134, 2009.
Riisgard, H. U., Kittner, C., and Seerup, D. F.: Regulation of opening state and filtration rate in

BGD
7, 5119–5156, 2010

filter-feeding bivalves (*Cardium edule*, *Mytilus edulis*, *Mya arenaria*) in response to low algal concentration, J. Exp. Mar. Biol. Ecol., 284, 105–127, 2003.

Roy, R. N., Roy, L. N., Vogel, K. M., Porter-Moore, C., Pearson, T., Good, C. E., Millero, F. J., and Campbell, D. M.: The dissociation constants of carbonic acid in seawater at salinities 5 to 45 and temperatures 0 to 45°C, Mar. Chem., 44, 249–267, 1993.

Thomsen, J. and Melzner, F.: Moderate seawater acidification does not elicit long-term metabolic depression in the blue mussel /Mytilus edulis/, Mar. Biol., submitted, 2010.

Weiss, R. F.: Carbon dioxide in water and seawater: the solubility of a non-ideal gas, Mar. Chem., 2, 203–215, 1974.

Yin, Y., Huang, J., Paine, M. L., Reinhold, V. N., and Chasteen, N. D.: Structural characterization of the major extrapallial fluid protein of the mollusc *Mytilus edulis*: implications for functions, Biochemistry, 44, 10720–10731, 2005.

BGD

7, 5119–5156, 2010

Table 1. Kiel Fjord surface seawater carbonate system speciation 2008 to 2009. Total alkalinity (A_T) and dissolved inorganic carbon (C_T) were measured by potentiometric titration using the VINDTA system and coulometric titration after CO_2 extration using the SOMMA system. Carbonate system speciation was calculated using the CO2SYS program. See Fig. 1a for corresponding surface pH_{NBS}.

#	Date	S	T (°C)	pH_{NBS}	A_T (µmol kg^{-1})	C_T (µmol kg^{-1})	pCO_2 (Pa)	pCO_2 (µatm)	Ω_{calc}	Ω_{arag}
1	09 Jul 2008	17.4	14.6	7.68	1955.2	1973.1	143	1411	0.79	0.47
2	13 Aug 2008	16.1	18.7	7.83	1913.7	1891.5	104	1026	1.21	0.72
3	08 Sep 2008	19.3	15.5	7.49	2044.9	2106.3	234	2309	0.58	0.35
4	15 Oct 2008	17.3	14.1	7.67	2018.4	2041.3	150	1480	0.79	0.47
5	11 Nov 2008	21.5	11.5	7.86	2063.3	2037.2	91	898	1.22	0.74
6	08 Dec 2008	19.6	7.1	7.98	2123.7	2088.2	68	671	1.34	0.80
7	12 Jan 2009	17.8	3.9	8.01	2078.3	2053.0	62	612	1.18	0.69
8	05 Feb 2009	16.5	3.3	8.10	2113.2	2075.3	52	513	1.36	0.79
9	05 Mar 2009	14.5	3.5	8.23	2067.7	2008.3	39	385	1.67	0.96

BGD
7, 5119–5156, 2010

Table 2. Seawater carbonate system speciation during experimental trials (mean±SD, 14 and 3 determinations for pH, S, T and A_T, C_T). Salinity (S) was 11.8±0.4 and temperature (T) 12.5°C±0.5°C in Exp. 1 (duration 2 weeks), T = 13.8°C±0.6°C and S=15.0±0.6 in Exp. 2 (duration: 8 weeks).

Treatment	pH_{NBS}	A_T (µmol kg^{-1})	C_T (µmol kg^{-1})	pCO_2 (Pa)	pCO_2 (µatm)	Ω_{calc}	Ω_{arag}
Exp. 1:							
39 Pa/385 µatm	8.05±0.03	1901.4±42.2	1841.5±36.2	47±2	464±20	1.77±0.13	1.01±0.08
57 Pa/560 µatm	7.89±0.04	1903.5±40.8	1873.5±31.3	67±5	661±49	1.31±0.16	0.75±0.09
85 Pa/840 µatm	7.81±0.03	1905.6±40.3	1891.8±34.7	80±3	789±30	1.09±0.09	0.62±0.05
113 Pa/1120 µatm	7.70±0.03	1906.2±38.9	1914.3±34.1	106±5	1046±49	0.86±0.07	0.49±0.04
142 Pa/1400 µatm	7.56±0.06	1906.1±39.3	1943.9±53.7	150±31	1480±306	0.64±0.09	0.37±0.05
405 Pa/4000 µatm	7.08±0.02	1890.8±25.1	2077.5±12.0	431±35	4254±345	0.22±0.01	0.12±0.01
Exp.: 2							
39 Pa/385 µatm	8.13±0.02	1966.1±3.2	1891.2±5.3	50±3	493±29	1.94±0.04	1.14±0.04
142 Pa/1400 µatm	7.72±0.06	1968.1±4.9	1984.4±12.3	135±20	1332±197	0.81±0.09	0.48±0.06
405 Pa/4000 µatm	7.26±0.04	1970.2±4.3	2125.8±12.6	395±22	3898±217	0.28±0.02	0.17±0.01

BGD
7, 5119–5156, 2010

Table 3. (A) Exp. 1 haemolymph acid-base status and ion concentrations of large mussels in relation to treatment pCO_2. Significant differences from control (39 Pa, 385 µatm treatment) in bold, mean values and SD. (B) Haemolymph (HL) vs. extrapallial fluid (EPF) acid-base status in 6 mussels from Kiel Fjord maintained for two weeks at a pCO_2 of ca. 50 Pa (ca. 500 µatm) in the experimental set-up (01–16 December 2008) at T=11.8 °C, S=19.4, pH_{NBS}=8.04.

a) experimental animal haemolymph acid-base status

Treatment (Pa/µatm)	pH_{NBS}	$[HCO_3^-]$ (mmol l^{-1})	$[CO_3^{2-}]e$ (µmol l^{-1})	pCO_2e (Pa)	pCO_2e (µatm)	$[Na^+]e$ % of SW	$[K^+]e$ % of SW	$[Mg^{2+}]e$ % of SW	$[Ca^{2+}]e$ % of SW
39 Pa/385 µatm	7.59±0.16	1.77±0.15	24.6±7.6	169.7±76.7	1675±757	100.9±1.9	128.9±15.2	104.4±2.0	110.5±6.7
57 Pa/560 µatm	7.53±0.15	1.78±0.13	22.4±7.4	171.8±90.6	1694±894	99.4±4.4	117.0±10.3	102.0±6.2	103.6±5.7
85 Pa/840 µatm	7.54±0.17	1.61±0.13	20.5±8.7	175.3±78.9	1730±779	103.3±5.9	120.7±18.2	105.9±6.0	109.1±8.4
113 Pa/1120 µatm	7.43±0.12	1.79±0.30	18.0±8.0	243.6±75.1	2404±741	102.5±2.7	130.4±7.3	102.7±5.4	106.3±5.4
142 Pa/1400 µatm	**7.36±0.11**	1.64±0.17	**13.6±2.4**	272.0±99.3	2684±980	102.9±2.4	130.4±25.9	103.6±5.4	110.3±4.2
405 Pa/4000 µatm	**7.16±0.09**	1.81±0.35	**9.8±3.9**	**496.0±31.8**	**4895±314**	**108.2±1.3**	134.8±11.5	108.2±1.2	113.1±2.6

b) haemolymph (HL) vs. extrapallial fluid (EPF) acid-base status

Fluid	pH_{NBS}	$[HCO_3^-]$ (mmol l^{-1})	pCO_2e (Pa)	pCO_2e (µatm)
HL	7.43±0.21	1.59±0.18	258±149	2546±1471
EPF	7.38±0.12	1.82±0.14	307±102	3029±1007

BGD
7, 5119–5156, 2010

Table 4. ANOVA results. (A) Exp. 1: one-factorial ANOVAs for extracellular acidbase and ion status of large mussels (factor: seawater pCO_2, pCO_{2sw}). Significant post-hoc tests ($p<0.05$, Tukey HSD) indicated in the manuscript figures and tables. Six seawater pCO_2 levels (39 to 405 Pa/385 to 4000 µatm), $N=12$ replictes for 39 to 142 Pa, $N=6$ replicates for 405 Pa. (B) Exp. 2: two-factorial ANOVAs (factors: seawater pCO_2 and initial size). Significant post-hoc tests ($p<0.05$, Tukey HSD) indicated in the manuscript figures and tables. Three seawater pCO_2 levels (39, 142 and 405 Pa/385, 1400 and 4000 µatm) and two size classes (small, medium), $N=4$ replicate aquaria for each treatment. (C) Exp. 2: one-factorial ANOVAs for shell microstructure (SEM) analysis of medium sized mussels (factor: seawater pCO_2, pCO_2sw). Significant post-hoc tests ($p<0.05$, Tukey HSD) indicated in the manuscript. Three seawater pCO_2 levels (39, 142, 405 Pa), $N=5$ replicate mussels analyzed. (D) Exp. 2: Kruskal-Wallis test results for comparison of shell dissolution area at the umbo and shell dissolution severity at the umbo vs. pCO_2 (39, 142, 405 Pa), $N=20$ replicate medium sized mussels analyzed. Significant Dunn's multiple comparison tests are indicated in Fig. 6.

A) Extracellular acid-base and ion status (Exp. 1)

	Factor	F	p
Extracellular pH	pCO_{2sw}	$F_{(5.56)}=172\,494$	**<0.001**
Extracellular $[HCO_3^-]$	pCO_{2sw}	$F_{(5.54)}=1.8$	>0.12
Extracellular $[CO_3^{2-}]$	pCO_{2sw}	$F_{(5.53)}=4.366$	<0.003
Extracellular pCO_2	pCO_{2sw}	$F_{(5.54)}=16.6874$	**<0.001**
Extracellular $[K^+]$	pCO_{2sw}	$F_{(5.55)}=1.67$	>0.15
Extracellular $[Na^+]$	pCO_{2sw}	$F_{(5.56)}=5.01$	**<0.001**
Extracellular $[Ca^{2+}]$	pCO_{2sw}	$F_{(5.56)}=2.28$	>0.05
Extracellular $[Mg^{2+}]$	pCO_{2sw}	$F_{(5.56)}=1.97$	>0.09

BGD
7, 5119–5156, 2010

Table 4. Continued.

B) Shell and somatic growth (Exp. 2)

	SS	Degr. Of Freedom	MS	*F*	*p*
a) shell length growth vs. seawater pCO_2 (pCO_{2sw}) and initial size (size)					
Intercept	6 436 372	1	6 436 372	7 864 467	0.000000
size	636 529	1	636 529	777 761	**0.000000**
pCO_{2sw}	16 563	2	8281	10 119	**0.001135**
size∗pCO_{2sw}	0.541	2	0.271	0.331	0.722615
Error	14 731	18	0.818		
b) dry mass growth vs. seawater pCO_2 (pCO_{2sw}) and initial size (size)					
Intercept	7.465.653	1	7.465.653	8.174.232	0.000000
size	3.838.226	1	3.838.226	4.202.520	**0.000000**
pCO_{2sw}	63.247	2	31.624	34.625	0.053424
size∗pCO_{2sw}	32.676	2	16.338	17.889	0.195616
Error	164.397	18	9.133		
c) shell mass growth vs. seawater pCO_2 (pCO_{2sw}) and initial size (size)					
Intercept	323 798.4	1	323 798.4	1 996 641	0.000000
size	160 413.0	1	160 413.0	989 156	**0.000000**
pCO_{2sw}	5566.3	2	2783.1	17.162	**0.000067**
size∗pCO_{2sw}	1930.4	2	965.2	5.952	**0.010375**
Error	2919.1	18	162.2		

BGD
7, 5119–5156, 2010

Table 4. Continued.

C) Shell microstructure (SEM) analysis (Exp. 2)

	Factor	F	p
Initial shell length	pCO_{2sw}	$F_{(2.12)}$=2.9	>0.09
Final shell length	pCO_{2sw}	$F_{(2.12)}$=0.1	>0.93
95% shell length: calcite thickness	pCO_{2sw}	$F_{(2.12)}$=0.85	>0.44
75% shell length: calcite thickness	pCO_{2sw}	$F_{(2.12)}$=1.45	>0.27
75% shell length: aragonite thickness	pCO_{2sw}	$F_{(2.12)}$=0.35	>0.70
75% shell length: number of aragonite layers	pCO_{2sw}	$F_{(2.12)}$=0.1	>0.91
75% shell length: thickness of aragonite layers	pCO_{2sw}	$F_{(2.12)}$=56.8	<**0.02**

D) Shell dissolution analysis (Exp. 2)

Group	*N* mussels	Sum of ranks	Mean of ranks
a) dissolution area at umbo vs. pCO_2			
39 Pa	20	35.5	1.8
142 Pa	20	64.6	3.2
405 Pa	20	83.0	4.2
Kruskal-Wallis Statistic=19.49, **p<0.0001**			
b) dissolution index at umbo vs. pCO_2			
39 Pa	20	36.7	1.8
142 Pa	20	56.9	2.8
405 Pa	20	89.5	4.5
Kruskal-Wallis Statistic=25.41, **p<0.0001**			

BGD
7, 5119–5156, 2010

Table 5. (Exp. 2): Shell microstructure analysis using SEM. N=5 mussels of similar final length (medium size) were cross sectioned at 75 and 95% shell length. Mean values and (SD), significant differences from control (39 Pa, 385 µatm) in bold. Both cross sections are located in parts of the shell that have been newly formed during the experimental incubation.

Treatment (Pa/µatm)	Initial shell length (mm)	Final shell length (mm)	95% shell length	75% shell length			
			calcite thickness (µm)	calcite thickness (µm)	aragonite thickness (µm)	Layers of aragonite (*n*)	aragonite layer thickness (µm)
39/385	12.4 (1.8)	21.4 (1.2)	95.6 (14.0)	99.2 (9.1)	9.6 (2.8)	15.8 (3.7)	0.60 (0.11)
142/1400	12.4 (1.3)	21,2 (0.9)	101.5 (17.3)	87.4 (6.0)	10.2 (6.2)	15.4 (6.8)	0.62 (0.13)
405/4000	14.1 (0.5)	21.1 (1.7)	109.6 (19.2)	99.7 (19.6)	7.5 (6.2)	17.2 (9.3)	**0.38 (0.13)**

BGD
7, 5119–5156, 2010

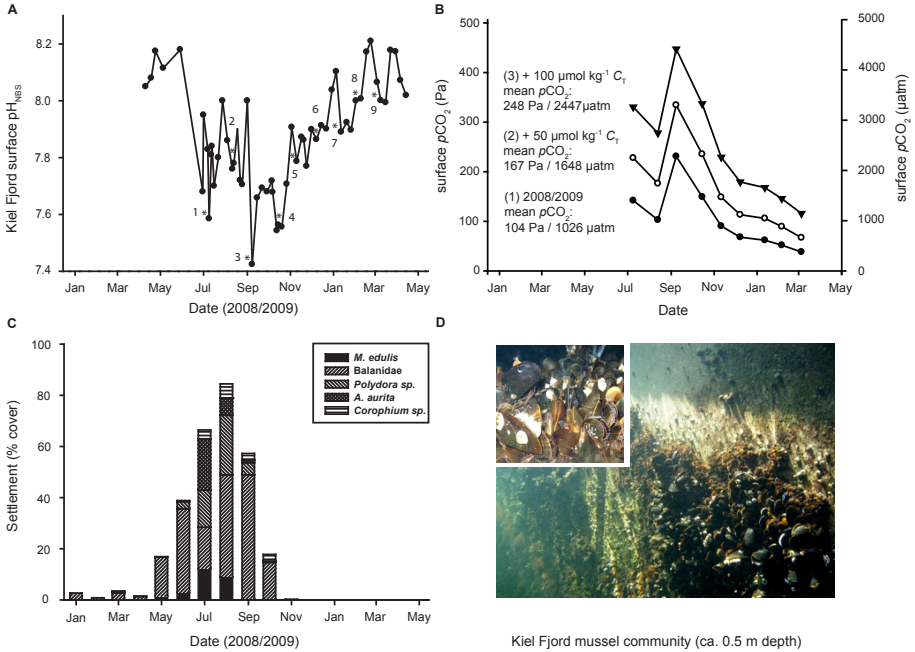

Fig. 1. **(A)** Surface pH_{NBS} in Kiel Fjord at the site of the experimental mussel population (54°19.8′ N; 10°9.0′ E) in 2008 and 2009. Stars and numbers indicate dates for which accurate determinations of total alkalinity (A_T) and dissolved inorganic carbon (C_T) are available, see Table 1. **(B)** Kiel Fjord pCO_2 replotted from Table 1, and calculated after addition of 50 (2) and 100 (3) µmol kg^{-1} of C_T to C_T from Table 1. A doubling in surface pCO_2 will result in an increase in C_T by about 90 µmol kg^{-1} in this habitat, see text. **(C)** Settlement of marine invertebrates on vertically suspended PVC plates. Plates (N=3 each) were exchanged monthly and aufwuchs was quantified. **(D)** Image of typical vertical hard substrate in Kiel Fjord dominated by calcifying communities.

BGD
7, 5119–5156, 2010

Calcifying invertebrates succeed in a naturally CO_2

J. Thomsen et al.

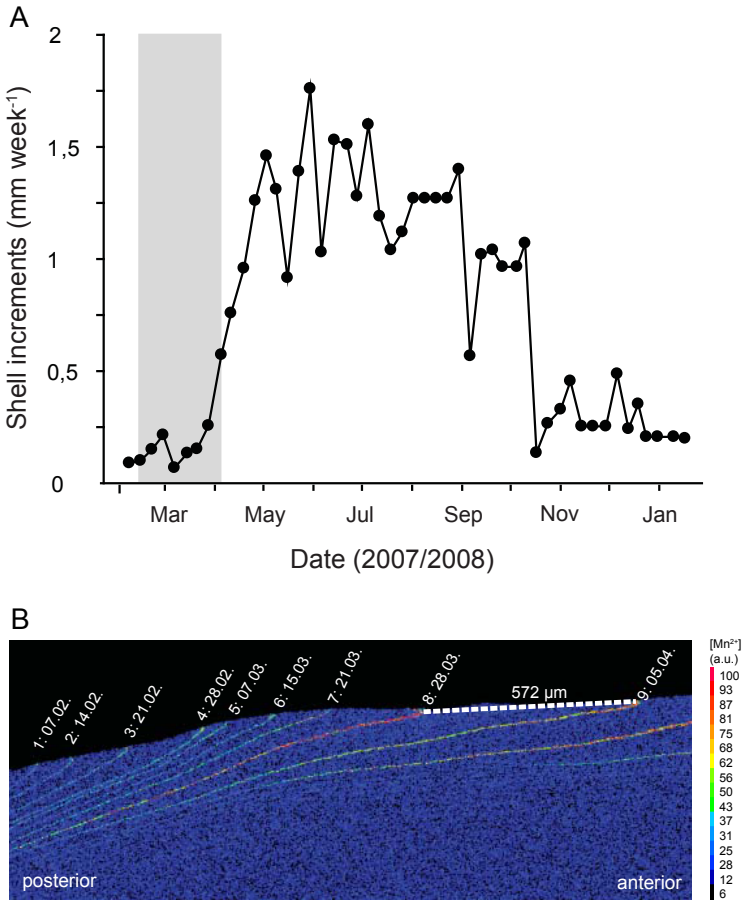

Fig. 2. Manganese marks in the calcite of the shell of a wild *Mytilus edulis* from Kiel Fjord illustrating weekly shell length growth between 07 February 2007 (line 1) and 05 April 2008 (line 9). Shell $[Mn^{2+}]$ in arbitrary units (a.u.). Grey bar in **(A)** indicates the time interval displayed in **(B)**.

BGD
7, 5119–5156, 2010

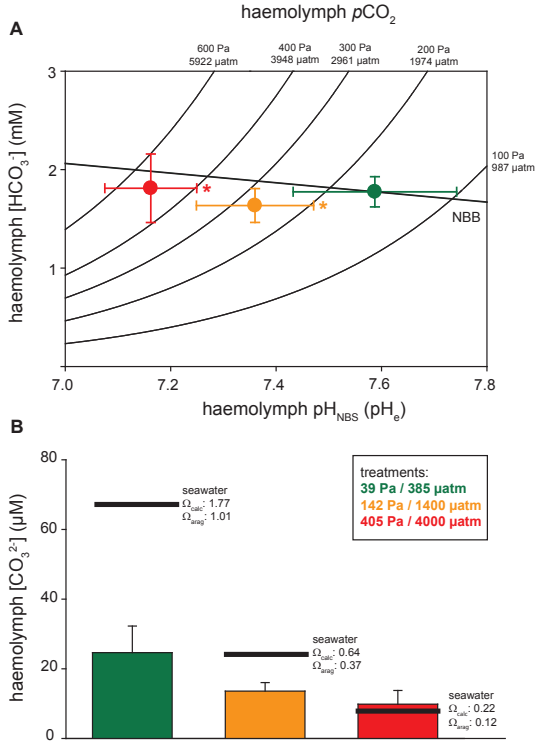

Fig. 3. (Exp. 1): **(A)** haemolymph acid-base status in relation to environmental pCO_2 (Davenport-diagram) for treatment groups under pCO_2 levels of 39 Pa (ca. 385 µatm, N=12), 142 Pa (ca. 1400 µatm, N=12) and 405 Pa (ca. 4000 µatm, N=6). Isobars represent haemolymph pCO_2. NBB=non-bicarbonate buffer line. Mussels cannot significantly elevate $[HCO_3^-]$ to compensate pH_e. See also Table 3 and Table 5 for ANOVA tables; **(B) (A)** Calculated haemolymph $[CO_3^{2-}]$ at seawater pCO_2 values of 39, 142 and 405 Pa (385, 1400, 4000 µatm). Black lines indicate seawater $[CO_3^{2-}]$ and the corresponding $CaCO_3$ saturation state (Table 4 for ANOVA tables).

BGD
7, 5119–5156, 2010

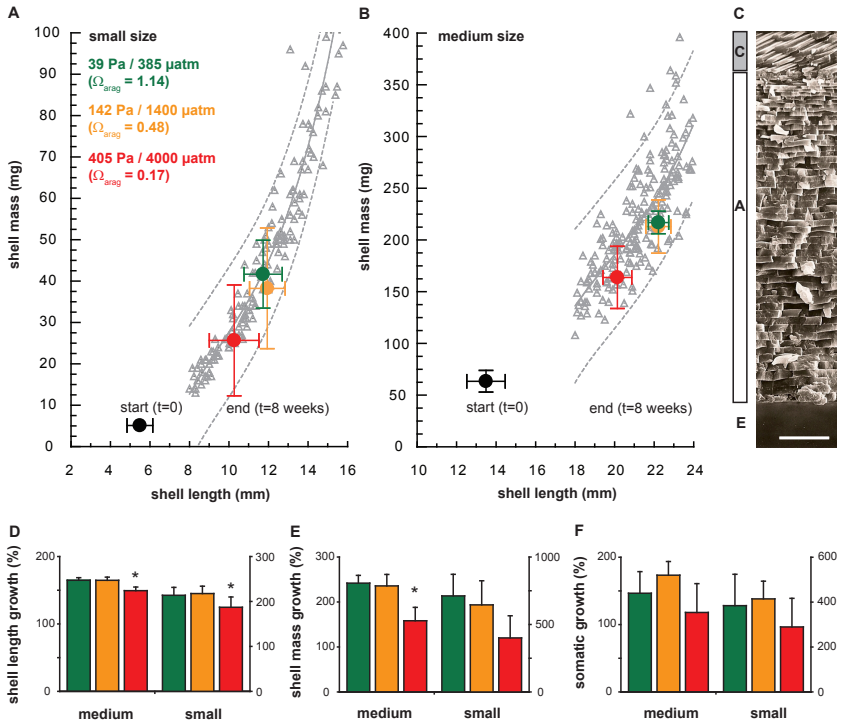

Fig. 4. (Exp. 2): (**A** and **B**): Shell mass vs. shell length relationships of small and medium experimental mussels at the beginning of the experiment (black) and after 8 weeks (red, orange, green; means and standard deviation). The grey symbols represent individual mussels from the collection site, the dashed line gives the 95% prediction interval for the shell mass vs. length relationship of wild mussels. **(C)**: SEM cross-section of *M. edulis* shell (detail), showing calcite **(C)** and aragonite **(A)** layers. Aragonite layers are in direct contact with the extrapallial fluid (EPF, E). Scale bar=10 µm. (**D**–**F**): Percent shell mass and length, as well as somatic (dry mass) growth over the entire 8 week period. See Table 4 for ANOVA tables.

BGD
7, 5119–5156, 2010

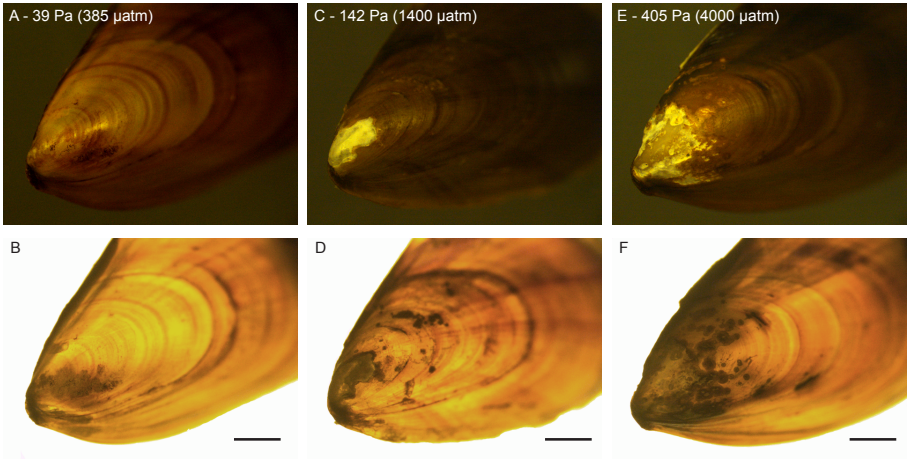

Fig. 5. (Exp. 2): External shell dissolution at the umbo region. Images of umbones of medium sized shells taken under reflected (**A**, **C**, **E**) and transmitted (**B**, **D**–**F**) illumination to quantify shell dissolution area and severity. In (**E** and **F**), dissolution spots are visible as darker regions, as corroded shell material blocks the light stronger than intact crystal structures. (**A** and **D**) 39 Pa (385 µatm), dissolution index=1, (**B** and **E**) 142 Pa (1400 µatm), dissolution index=2, (**C** and **F**) 405 Pa (4000 µatm), dissolution index=3; scale bars=2.5 mm.

BGD
7, 5119–5156, 2010

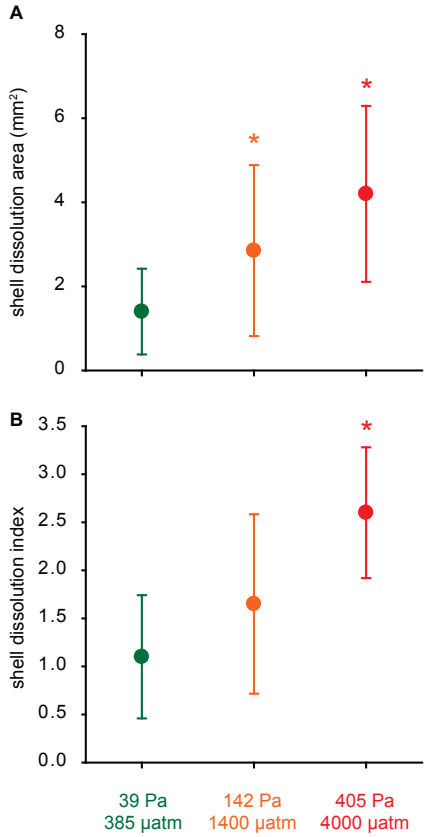

Fig. 6. (Exp. 2): **(A)** shell dissolution area at the umbo region (mm^2) of medium sized mussels, **(B)** shell dissolution index; N=20 mussels randomly chosen from the 4 replicate treatments, asterisks indicate significant differences from control (39 Pa, 385 µatm) using Dunn's test. See Table 4 for Kruskal-Wallis test results.

BGD
7, 5119–5156, 2010

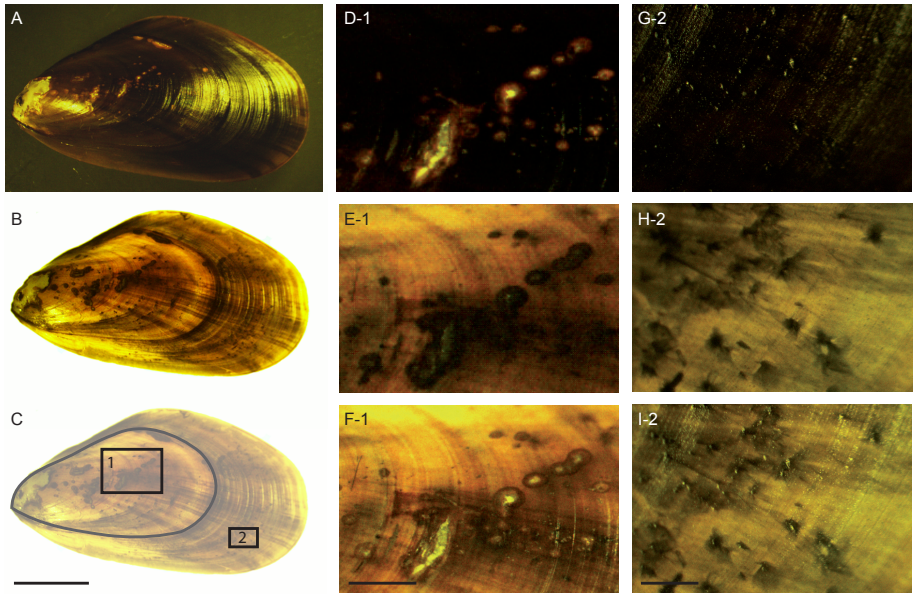

Fig. 7. (Exp. 2): Example of a medium sized mussel (405 Pa, 4000 µatm) with dissolution spots on old and newly formed parts of the shell. (**A**–**C**) overview, reflected light (A), transmission light (B), position of close-up areas 1 and 2 (C) which are depicted in (**D**–**I**). Close up area 1 (D–F) is located on pre-experimental shell parts (black trace in (C) indicates the size of the mussel at the start of the experiment), close-up area 2 (G–I) on newly formed shell material. (D and G) are reflected light pictures, (E and H) are transmission images, (F and I) combined reflected and transmission images. White spots are corroded calcite material that is visible when the periostracum is fractured. These spots appear dark when viewed under transmission light. Scale bars: (A–C) 5 mm, (D–F) 1 mm, (G–I) 0.5 mm.

BGD
7, 5119–5156, 2010